Tunable Resonant Raman Scattering From Singly Resonant Single Wall Carbon Nanotubes

Yan Yin, *Student Member, IEEE*, Andy G. Walsh, A. Nick Vamivakas, Stephen B. Cronin, Alexander (Sasha) M. Stolyarov, Michael Tinkham, Wolfgang Bacsa, M. S. Ünlü, *Senior Member, IEEE*, Bennett B. Goldberg, *Member, IEEE*, and Anna K. Swan, *Member, IEEE*

***Abstract*—We perform tunable resonant Raman scattering on 17 semiconducting and seven metallic singly resonant single wall carbon nanotubes. The measured scattering cross section as a function of laser energy provides information about a tube's electronic structure, the lifetime of intermediate states involved in the scattering process, and also the energies of zone center optical phonons. Recording the scattered Raman signal as a function of tube location in the microscope focal plane allows us to construct two-dimensional spatial maps of singly resonant tubes. We also describe a spectral nano-scale artifact, which we have termed as the "nano-slit effect."**

***Index Terms*—Carbon nanotube, excitons, Raman scattering.**

I. Introduction

CARBON nanotubes represent prototypical one-dimensional (1-D) systems that are under intense study not only for their intrinsic physical properties, but also for their potential applications as transistors, sensors, and opto-electronic devices. The electronic properties exhibited by these systems depend sensitively on the tube structure, characterized by two integers (n and m) that determine whether a single wall carbon nanotube (SWNT) will exhibit electronic properties characteristic of either an insulator or a metal [1], [2]. Typical of 1-D structures, SWNTs exhibit sharp van Hove singularities in the electronic density of states (DOS). To date, a number of photoluminescence (PL) studies have been utilized to probe the rich excitation spectrum of single SWNTs [3]–[5]. More recently, two-photon absorption combined with one-photon emission PL studies on isolated tubes has verified theoretical predictions of the excitonic nature of the electronic excitation spectrum of semiconducting SWNTs [6]–[9]. The band-edge absorption is suppressed and almost the entire oscillator strength is transferred to the lowest exciton level, as is typical for absorption in 1-D systems [10], [11]. As the lowest exciton, for a given subband pair, carries the majority of the oscillator strength, it is still useful to refer to the optical transition associated with the valence and conduction subbands j as E_{jj}.

In addition to PL, Raman scattering is another widely used spectroscopy technique for SWNT characterization [12]. In contrast to the PL studies, there is a direct correlation between the incoming and the outgoing photons in Raman scattering. Specifically, energy and momentum conservation dictate that the laser frequency is equal to the sum (difference) of the scattered laser and emitted (absorbed) phonon frequencies and that the laser momentum is equal to the sum (difference) of the scattered photon and phonon momentums. Raman signal is resonantly enhanced when the incoming or scattered photon energy is commensurate with the energy of an electronic excitation. The sensitivity of Raman scattering to both a material's phonons and electronic excitations makes it a useful tool for studying how these quasi-particles couple to external parameters controllable by the experimenter, e.g., strain [13], temperature dependence [14], [15], and changing environment [16]–[18]. In addition, Raman scattering also allows measurements from metallic tubes, inaccessible in PL measurements [17], [19], [20].

In this paper, we have employed a tunable laser source to conduct the Raman scattering measurements on singly resonant SWNTs suspended in air. By singly resonant tubes we mean that signal is collected only from one resonant tube, although non-resonant tubes might be present in a small bundle with the resonant tube. The tunable light source permits us to measure the resonance excitation profile (REP) of a singly resonant nanotube. The REP measures the Raman scattered intensity as a function of laser frequency. The spectral location of the REP yields information about the SWNT's electronic structure. It is also possible, using the relative heights of different REPs, to quantify electron–phonon coupling strengths [21]. Finally, the width of the REP provides information about the lifetimes of the intermediate states that participate in the Raman scattering process. In addition, the resonant Raman signal can be used as a means to provide two-dimensional (2-D) images of our SWNT samples.

II. Resonant Raman Scattering

In SWNTs, one-phonon resonant Raman scattering is used as a probe of the tube's vibrational and electronic excitation

Manuscript received April 3, 2006; revised August 13, 2006. This work was supported in part by the National Science Foundation under Grant ECS 0210752 and in part by a Boston University SPRInG grant.

Y. Yin, A. G. Walsh, A. N. Vamivakas, and B. B. Goldberg are with Boston University, Boston, MA 02215 USA (e-mail: yanyin@bu.edu; h46av8r@bu.edu; nvami@bu.edu; Goldberg@bu.edu).

S. B. Cronin was with Harvard University, Cambridge, MA 02138 USA. He is now with the Department of Electrical Engineering—Electrophysics, University of Southern California, Los Angeles, CA 90089 USA (e-mail: scronin@usc.edu).

A. M. Stolyarov and M. Tinkham are with Harvard University, Cambridge, MA 02138 USA (e-mail: stolyar@fas.harvard.edu; tinkham@rsj.harvard.edu).

W. Bacsa was on sabbatical leave from Boston University. He is with Universite Paul Sabatier, 31062 Toulouse, France (e-mail: wolfgang.bacsa@lpst.ups-tlse.fr).

M. S. Ünlü and A. K. Swan are with the Department of Electrical and Computer Engineering, Boston University, Boston, MA 02215 USA (e-mail: selim@bu.edu; swan@bu.edu).

Digital Object Identifier 10.1109/JSTQE.2006.883694

spectrum and to provide information about the tube's structural properties. Specifically, the SWNT's radial breathing mode (RBM) frequency gives a direct measure of the nanotube diameter [22], [23]. To quantify the strength of the measured Raman scattered signal, we use the differential Raman scattering cross section [24]

$$\frac{d\sigma(\omega_l;r)}{d\Omega} = A(r)\beta_{s/AS} \times \left| \frac{1}{\sqrt{\hbar\omega_l \mp \hbar\Omega_p - E_{jj} - i\eta}} - \frac{1}{\sqrt{\hbar\omega_l - E_{jj} - i\eta}} \right|^2 \quad (1)$$

where $h\,\omega_l$ is the exciting photon frequency, $h\,\Omega_p$ is the phonon mode energy, E_{jj} is the energy of the electronic excitation mediating the scattering process, η is the parameter that quantifies the intermediate state's lifetime, the $\mp$ corresponds to phonon creation ($-$, Stokes) or phonon annihilation ($+$, anti-Stokes), A is the product of constants and matrix elements, r is the location along the SWNT, and $\beta_{\mathrm{S/AS}}$ is the Boltzmann factor with $\beta_{\mathrm{AS}} = \exp[-\Omega_p/kT]$ for anti-Stokes scattering and $\beta_S = 1$ for Stokes scattering. A resonance in the scattering cross section is a result of either of the two real parts of the energy denominators in (1) tending to zero. Examination of (1) reveals that this can happen in two distinct cases. The first possibility is that the exciting laser photon has an energy that is equal to an electronic transition energy in the system. When the "incoming" resonance occurs, the scattered signal strength is greatly enhanced. Enhancement is also observed in the case of an "outgoing" resonance when the scattered photon energy is equal to an electronic transition energy ($\hbar\omega_s = \hbar\omega_l \mp \Omega_p$).

In (1), we have made explicit the scattering cross-section dependence on both the exciting laser frequency and the specific position along the tube that is excited. Equation (1) is derived ignoring finite beam size effects, and we have artificially introduced the position index r to illustrate the ability to measure the Raman scattered light from different tube locations. This has been illustrated beautifully in the work by Hartschuh *et al.* [25], who used tip-enhanced Raman scattering achieving nm scale lateral resolution. In Section III, we study the scattering cross section for a specific phonon mode as a function of location along the tube, albeit with diffraction limited optical resolution, which still reveals much about the sample. Using the scattered laser light, we can construct an image of the tube that is correlated with a specific phonon mode. In Section IV, the differential scattering cross section as a function of laser frequency ω_l, the REP, is studied. Using the REP, we are able to identify the specific electronic transition energies E_{jj}, identify the specific phonon mode energies $\hbar\Omega_p$, estimate the intermediate state's lifetime η, and determine the SWNT temperature from $\beta_{\mathrm{S/AS}}$.

Implicit in (1) is the assumption that the intermediate electronic states participating in the Raman scattering process are free electrons and not excitons, but the qualitative features in these two cases of the REP are the same [26], and the measured E_{jj} can be reinterpreted as the exciton energy. It is worth noting that the asymmetry in the van Hove singularities from the free-electron band would not result in an asymmetric REP line shape [27]. Specifically, Section IV illustrates the measured REPs as indeed the symmetric functions of the excitation laser frequency.

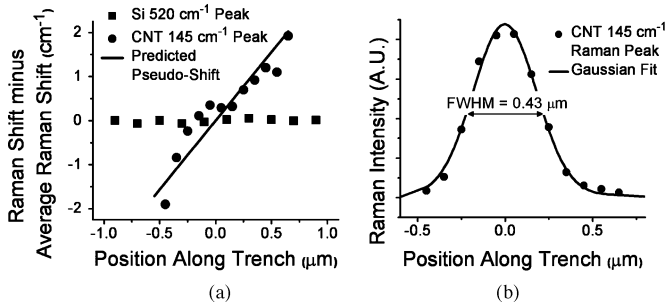

Fig. 1. (a) Measurement of the "pseudo-shift" in Raman frequency when the nanotube is translated along the spectral direction in the object plane. The *solid line* is the calculated shift based on the optical system parameters. The *square points* from a Si surface illustrate that for a macroscopic object, there is no "nano-slit" effect. (b) Nanotube provides the means to measure the FWHM of the focused spot.

A. Artifacts in Spectroscopy of Nano-Scale Objects

It is well known that even a spectrally sharp signal such as a Raman line or a laser line will appear broadened in energy unless a slit in the intermediate image plane at the entrance to the spectrometer is used to limit the collection from off-axis points. Only the emission from precisely that point in the object plane that lies on the optical axis will map to the exact center of the correct pixel on the detector. In a spectrometer, the diffraction grating defines the spectral direction in the detector array and in the object plane. When the emitter is of nano-scale dimension, i.e., effectively a point source in the object plane and located slightly off the optical axis in the spectral direction, this effect leads not to broadening but rather to false spectral shifts. Knowing the resolution of the spectrometer, detector pixel size, and the overall magnification from object plane to detector, this "pseudo-shift" is easily calculated for a given distance in the spectral direction of the emitter from the optical axis. For these reasons, it is important to ensure that the nanotube bisects the optical axis perpendicularly and is aligned parallel with the spectral direction. In this way, the spectrum that derives from the light originating from along the length of the nanotube is not artificially broadened or shifted. We refer to this as the "nano-slit effect," i.e., the nanotube acts as a point emitter with respect to the spectral direction and as an extended object in the nonspectral direction.

The "nano-slit" effect is illustrated by measuring the shift RBM frequency as a function of position steeping across the nanotube oriented parallel to the groove direction of the spectrometer grating. At the used wavelength, the spectrometer resolution is 2.4 cm^{-1} per pixel, the pixel size is 22 μm, and the magnification from object to image plane is $28.8\times$. This translates to a 3.1 cm^{-1} pseudo-shift for every micron the emitter is off-axis in the spectral direction. In Fig. 1(a), a nanotube is translated in the spectral direction in 100-nm steps with spectra

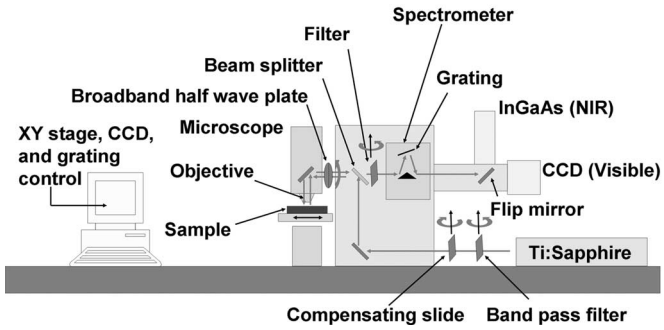

Fig. 2. Schematic drawing of the experimental setup.

taken at each point while the beam spot remains along the optical axis. The spectral deviations of the RBM from its on axis value are plotted in Fig. 2(a) with circles. The solid line shows the calculated slope of 3.1 cm^{-1} per micron. For comparison, the spectral deviation of the silicon 520 cm^{-1} Raman peak from the substrate is also shown. The silicon signal originates from all points illuminated by the beam spot and is unaffected by translation and consequently does not shift with sample position. However, the silicon line will be artificially broadened for the reasons outlined above.

The "nano-slit" configuration also provides an elegant method for directly measuring the profile of the beam intensity in the object plane. With the beam spot aligned (and fixed) along the optical axis, the stage, and hence the nanotube, is stepped in small increments through the beam. Knowing the orientation of the nanotube, as explained earlier, one can ensure that the nanotube is moved in a direction perpendicular to its length. The length of the tube will then effectively integrate the beam intensity along the direction perpendicular to the direction of motion. An example is shown in Fig. 1(b) with 100-nm steps, 807-nm excitation, and a $100\times/0.9$ numerical aperture (NA) objective. The theoretical single-point resolution predicted by a paraxial and scalar theory of light focusing 0.51 λ/NA is 0.457 μm. A Gaussian profile is used to fit the data and yields a full-width at half-maximum (FWHM) of 0.43 μm. The discrepancy in the measured resolution when compared to the theoretical prediction can be explained by the large NA vector field theory of light focusing. Richards and Wolf [28] first predicted that the FWHM of strongly focused light in the direction perpendicular to the illumination light polarization will be decreased when compared to the predictions of a scalar paraxial theory. Using the vector field theory, assuming plane wave illumination of the objective back aperture, yields an FWHM of 0.419 μm, which is in good agreement with our measurement. The slightly larger value measured is due to the finite width of the laser beam on the objective back aperture.

III. Experimental Configuration

The system layout is shown in Fig. 2. A tunable continuous wave (CW) Ti–sapphire laser is used for Raman excitation in the range 720–830 nm. The Raman spectrometer is a Renishaw 1000B modified to allow for tunable laser line rejection by tilt-tuning of two sets of overlapping filters. An 830-nm edge filter (Iridian Spectral Technologies) is angle tuned from 770 to 830 nm and a 785-nm holographic notch filter (Kaiser Optical Systems, Inc.) is angle tuned from 720 to 785 nm with some sacrifice in optical density for higher angles. A broadband half-wave plate is used to rotate the polarization of the incident beam in the object plane parallel to the nanotube axis as determined by maximizing the Raman peak intensity. The wave plate is intentionally placed between the microscope and the spectrometer so that the signal, also polarized parallel to the nanotube, is then rotated back to a consistent plane of polarization (P). This alleviates the need to correct for the polarization dependencies of a number of components, such as the filter and grating. This is important since the spectral position of the long pass edge or of the notch is different for S and P polarizations for non-normal incidence. The laser beam is focused by a $100\times$ objective with the Gaussian spot-profile FWHM $= 0.47$ μm and $E_{\text{laser}} = 785$ nm (Fig. 1). The typical excitation laser power used is less than 3 mW and direct measurements of Stokes and anti-Stokes intensity ratios show that no heating of the nanotubes takes place under such powers [29]. A 600 groove/mm grating optimized for near-infrared wavelengths yields a spectral resolution of ~ 2.8 cm^{-1} on the Si-charged coupled device camera. Compared to a triple monochromator, the use of filters and a single grating offers a high-throughput system enabling single-tube Raman signal detection.

To avoid interactions with the substrate, we use samples with nanotubes suspended across etched trenches on quartz substrates. The samples are prepared by first etching a set of trenches that varies in width from 1 to 2 μm with fiduciary markers to make it possible to locate a specific nanotube repeatedly in the optical microscope. SWNTs are grown over trenches by chemical vapor deposition [30] that produces nanotubes with a range of diameters. We focus on nanotubes from approximately 0.9 to 1.2 nm. In order to find a resonant carbon nanotube, the microscope stage is scanned to probe along a 77-μm long trench on the sample and typically three to ten resonant tubes are found in each trench. (Stokes RBM peak count rates are 30–350 counts/s). Depending on the details of the growth parameters, we have samples of relatively high-carbon nanotube density as well as low-density samples, shown in Figs. 3(a) and 4(a), respectively.

A. Higher Density Samples

The scanning electron microscope (SEM) image in Fig. 3(a) illustrates the somewhat chaotic growth observed in the high-density samples. From these samples, more than one resonant tube can often be observed in a single Raman spectrum, as shown by the multiple RBMs seen in Fig. 3(b). Based on a single spectrum, it is difficult to tell if the signal comes from two tubes that are combined in a small "rope" or if it comes from two individual tubes that both are within the FWHM of the laser spot. However, one can acquire more information about the geometry of the tube arrangements by the use of "hyperspectral" imaging by spatially mapping a larger area, and recording a Raman spectrum for each position. This is illustrated in Fig. 3(b)–(f). Fig. 3(b) shows a Raman spectrum from a

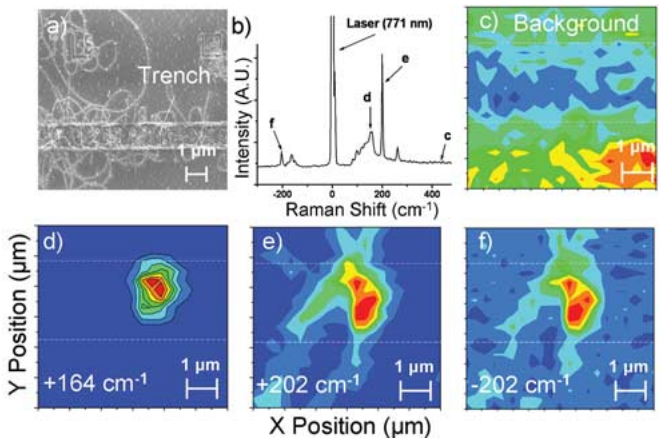

Fig. 3. SEM and Raman images of the high-density sample. (a) SEM image of a high-nanotube-density sample. (b) Raman spectrum from the center of the trench. Several RBM peaks indicate many tubes are resonant within the beam. The marked peaks are imaged in (c), (d), (e), and (f). (c) Elastically scattered background from the laser and the outline of the trench. (d) RBM from a metallic nanotube. (e) and (f) Crossing of identical nanotubes imaged via the Stokes and anti-Stokes RBM.

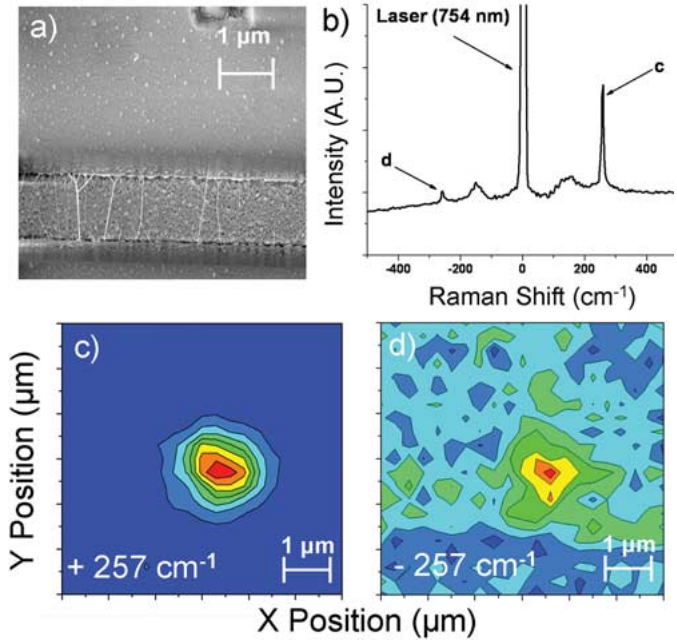

Fig. 4. SEM and Raman images of the low-density sample. (a) SEM image. (b) Raman spectrum from the center of the trench. Only one RBM peak indicates a singly resonant nanotube is present in the beam. (c) and (d) Scanned images of the Stokes and anti-Stokes RBM Raman peak, respectively. Typical of these samples signal is only found over the trench.

specific location along the trench. The spectrum shows several RBM peaks on the Stokes side, labeled d and e, and an associated anti-Stokes peak f, which corresponds to peak e on the Stokes side. Maps can be made displaying the intensity of any chosen Raman frequency, and four such maps are shown in Fig. 3(c)–(f), corresponding to the Raman shifts labeled c–f in the Raman spectrum in Fig. 3(b). The color scale gives the intensity of the mapped Raman signal. Fig. 3(c) shows the background signal from the elastically scattered laser light, showing the outline of the trench visible due to different focal conditions of the flat substrate and the trench. Fig. 3(d) shows the spatial map of a metallic nanotube with $\Omega_{\mathrm{RBM}} = 164$ cm^{-1}, with a small spatial extent. Fig. 3(e) and (f) shows Stokes and anti-Stokes maps of two semiconducting tubes of the same chirality ($\Omega_{\mathrm{RBM}} = 202$ cm^{-1}) crossing each other as they span the trench. We note that the signal is strongest from the suspended part of the nanotubes, which we have consistently observed.

Different maps illustrate that for this particular sample, the resonant nanotubes are close to each other but do not form a rope. The two identical semiconducting tubes cross each other, and the small spatial extent of the resonant signal from the metallic tube indicates that either it is short and does not span the width of the trench, or that it is only suspended closer to the upped edge of the trench before it comes in contact with the bottom of the trench.

B. Lower Density Samples

Fig. 4(a) shows an SEM image of a typical low-density sample. The common characteristics of these samples are that the nanotube growth starts and ends at the edge of the trench, and cross nearly at right angles to the trench. Furthermore, nanotubes are bundled together into small ropes of approximately two to five nanotubes while some nanotubes appear to be individual. As we will see from the resonant Raman excitation profiles, whether the nanotube is single or roped affects both the resonance energy and the coupling to the intermediate states as evidenced by the broadening of the resonance Raman excitation profile. The Raman spectrum in Fig. 4(b) shows signal only from one resonant nanotube (n, m) species shown by the single RBM mode visible at $\Omega_{\mathrm{RBM}} = 257$ cm^{-1}. The shoulders on either side of the laser line are due to incomplete blocking of the laser line by the angle-tuned filter. Fig. 4(c) and (d) shows the Stokes and anti-Stokes 257 cm^{-1} Raman peak height as a function of position.

IV. Resonance Excitation Profiles of Singly Resonant Carbon Nanotubes

In this section, we investigate a series of singly resonant SWNTs with different diameters and chiralities, suspended over trenches in air and record their resonant Raman excitation profiles. The procedure to find a singly resonant tube for study is described in Section III. The REPs of resonant SWNTs are measured by recording a Raman spectrum from a singly resonant tube over a range of excitation laser wavelengths (730–830 nm) in 4-nm steps while maintaining a constant excitation power (< 3 mW). Each individual Raman spectrum is corrected for the Si CCD quantum efficiency curve for different photon wavelengths. Furthermore, each profile is measured twice to ensure repeatability, with the excitation wavelength staggered 2 nm between the two runs, respectively. Fig. 5 shows the raw spectral data map (with background subtracted) of the anti-Stokes (AS, left) and Stokes (S, right) from a tube with an RBM ($\Omega_{\mathrm{RBM}} = 258$ cm^{-1}). Each horizontal line is a single Raman spectrum of the RBM peak at a particular excitation energy given by the ordinate axis. The resonant behavior of the Raman

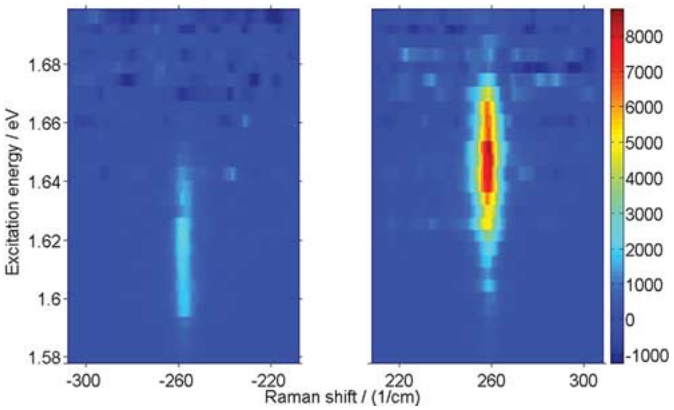

Fig. 5. Resonant Raman excitation maps. (a) Excitation energy dependence of the anti-Stokes RBM intensity. (b) Excitation energy dependence of the Stokes RBM intensity. Note the different intensity scales for the S and AS resonance, as well as the shift in resonance energy. The maps show the strong resonant behavior of the Raman intensity.

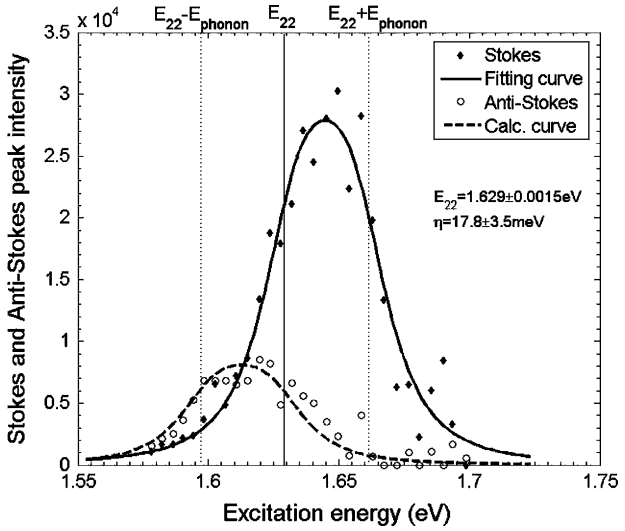

Fig. 6. Resonance excitation profiles for the Stokes and anti-Stokes maps in Fig. 5. The S REP is fit using (1), and E_{22} and η are extracted. The same values of the parameters are used to calculate the anti-Stokes scattering profile, after changing the sign for the phonon energy and using $\beta_{\mathrm{S,AS}}$.

intensity is evident from Fig. 5. The S and AS intensity maxima are shifted in the excitation energy by the RBM phonon energy due to the resonant enhancement for both the "incoming" and the "outgoing" resonant photons described in Section II.

To construct the REP from the map, the Raman peak intensity for each spectrum is plotted versus the laser energy. The peak intensity is obtained by integrating the Raman intensity in a ± 15-cm^{-1} wide window centered on Ω_{RBM} after subtracting a linear background. The resulting REPs from the AS and S RBM peaks are shown in Fig. 6, where the solid curve is a fit to the measured Stokes resonance profile using (1) of Section II, which determines both the broadening η and the resonance energy E_{22}^S (in E_{jj}^X, j are the valence and conduction subbands involved in the transition and X is either S for semiconductor or M for metal). The fit of the Stokes REP shown in Fig. 6 yields $E_{22}^S = 1.629$ eV ± 1.5 meV and $\eta = 17.8 \pm 3.5$ meV. The ver-

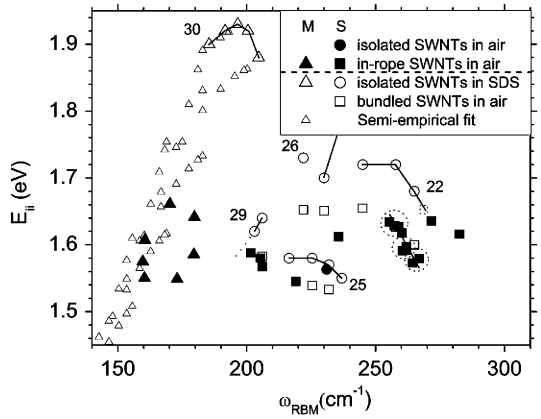

Fig. 7. Experimental plot of E_{ii} versus ω_{RBM} for the 18 semiconducting SWNTs (*filled squares*) and seven metallic SWNTs (*filled triangles*) measured in air, and for comparison, in SDS [17] and a semi-empirical fit for metallic SWNTs [31]. The *filled circle* in branch 22 is the only individual semiconducting tube. The numbers denote the $2n + m$ branches. The horizontal lines indicate our experimentally measurable range for excitation photon energy.

tical lines show the "incoming" (solid) and "outgoing" (dotted) resonances. The dashed line in Fig. 6, the anti-Stokes resonance profile, is *calculated* from (1) using E_{22}^S and η determined from the Stokes fit. The magnitude of the AS profile is scaled by the Boltzmann factor $e^{-\Omega_p/kT}$ with Ω_p = 258 cm^{-1} (the RBM frequency) and the nanotube temperature assumed equal to 300 K. The agreement between the calculated (dashed line) and measured (open circles) AS resonance profiles in Fig. 6 are striking. This not only demonstrates that the nanotube remains at room temperature (300 K) and suffers negligible laser heating, but also that it is possible to accurately extract resonance energies and broadening parameters from the measured REPs using (1). Measurements of nanotubes in dry nitrogen atmosphere, before and after heating, exhibit the same resonance energy as nanotubes in air [14]. Hence, we see no trace of water adsorbed on the nanotubes in air, probably due to the hydrophobic nature of graphite. Repeated measurements on the same nanotube on different occasions gave the same resonance energy within a few millielectronvolts.

V. Result

Results from all the 24 measured REPs are plotted in Fig. 7 compared to data from ensembles of individual tubes in solution [17], [31]. We use the previous PLE and resonant Raman studies of ensembles of individual nanotubes in solution to guide in the (n, m) assignment of the nanotubes studied in this work [5], [17].

Our experimental results for most of the nanotubes displayed as filled squares in Fig. 7 are 70–90 meV lower than for SWNTs suspended in SDS solution. The resonance energies measured are closer to the energies found from nanotubes in bundles than from nanotubes in SDS solution [17]. Rayleigh scattering measurements of carbon nanotubes suspended across wide trenches has also shown a downshift in the resonance energy by $\sim$10 s meV when a second nanotube joins the single nanotube [32]. For all cases but one (the filled circle in Fig. 7),

TABLE I
TWENTY-FOUR MEASURED NANOTUBES. THE ENERGIES IN "REPORTED RESULTS" ARE FROM [17], WHERE E'_{22} IS FROM NANOTUBES SUSPENDED IN SDS SOLUTION AND E''_{22} IS FROM NANOTUBES IN LARGE BUNDLES. "DIFFERENCES" COMPARE OUR MEASURED ENERGIES E_{22} WITH E'_{22} AND E''_{22} AND SHOW VERY SIMILAR VALUES WITH THE NANOTUBES IN BUNDLES

CVD grown SWNTs (this study)					Reported results			Differences	
SWNTs	ω_{RBM} (cm^{-1})	η (meV)	E_{22} (eV)	(n,m)	ω'_{RBM} (cm^{-1})	E'_{22} (eV)	E''_{22} (eV)	$\Delta E'_{22}$ (meV)	$\Delta E''_{22}$ (meV)
1	159.7	25±6	1.575±0.003	M	n/a	n/a	n/a	n/a	n/a
2	160.3	40±7	1.550±0.003	M	n/a	n/a	n/a	n/a	n/a
3	160.5	28±5	1.607±0.003	M	n/a	n/a	n/a	n/a	n/a
4	170.2	49±7	1.661±0.003	M	n/a	n/a	n/a	n/a	n/a
5	173.0	16±4	1.549±0.002	M	n/a	n/a	n/a	n/a	n/a
6	179.5	24±10	1.585±0.004	M	n/a	n/a	n/a	n/a	n/a
7	179.7	14±4	1.641±0.002	M	n/a	n/a	n/a	n/a	n/a
8	201.5	21±6	1.587±0.003	13,3	203.0	1.62	n/a	-33	n/a
9	205.3	9±5	1.580±0.003	14,1	206.0	1.64	1.58	-60	0
10	206.0	15±10	1.567±0.004	14,1	206.0	1.64	1.58	-73	-13
11	219.0	27±7	1.545±0.003	9,7	216.4	1.58	n/a	-35	n/a
12	231.0	45±8	1.562±0.003	11,3	231.9	1.57	1.53	-8	+32
13	235.7	27±11	1.612±0.005	n/a	n/a	n/a	n/a	n/a	n/a
14	255.3	18±9	1.634±0.004	9,4	257.8	1.72	1.63	-86	+4
15	257.3	18±4	1.629±0.001	9,4	257.8	1.72	1.63	-91	-1
16	259.0	19±4	1.627±0.002	9,4	257.8	1.72	1.63	-93	-3
17	260.2	23±10	1.618±0.004	n/a	n/a	n/a	n/a	n/a	n/a
18	260.5	16±4	1.591±0.001	10,2	265.0	1.68	1.60	-89	-9
19	261.8	16±7	1.597±0.003	10,2	265.0	1.68	1.60	-83	-3
20	261.8	10±5	1.592±0.002	10,2	265.0	1.68	1.60	-88	-8
21	264.3	13±8	1.573±0.004	11,0	266.7	1.657	n/a	-84	n/a
22	267.0	13±3	1.579±0.001	11,0	266.7	1.657	n/a	-78	n/a
23	271.7	27±22	1.636±0.010	n/a	n/a	n/a	n/a	n/a	n/a
24	282.5	24±5	1.616±0.002	n/a	n/a	n/a	n/a	n/a	n/a

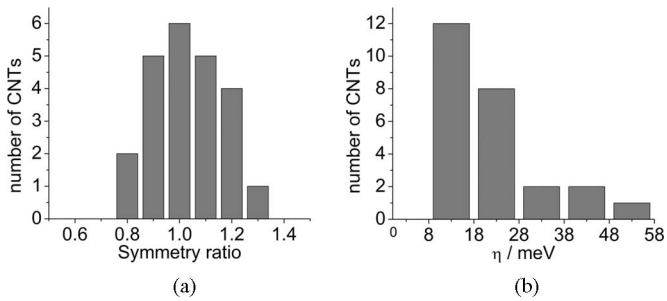

Fig. 8. (a) Bar diagram of the experimentally measured symmetry of the REPs. (b) Most nanotubes have a broadening factor η below 28 meV, and these tubes have been identified as nanotubes in small ropes.

the comparison gives close agreement with the energies for nanotubes in bundles. Combining the agreement of our measurements with the bundled tube data, the SEM data in Fig. 4(a) shows a preponderance of small nanotube ropes (two to five nanotubes), and by the lack of PL signal from our tubes, we conclude the nanotubes with down-shifted energies are indeed the result of the nanotubes forming small ropes.

Table I compiles all the data measured on our 24 nanotubes compared with previous measurements of tubes in solution and bundles [17]. Specifically, we report the RBM frequencies Ω_{RBM}, the measured linewidth broadening η, the electronic transition energy E_{22}^{X}, and the chirality assignments (n, m).

In addition to tube assignments, we used the 24 measured REPs to quantify the REP symmetry. Specifically, we defined a symmetry ratio $R = I_{\mathrm{above}}/I_{\mathrm{below}}$, where I_{above} (I_{below}) is the integrated spectral intensity for all laser frequencies above (below) the center of the fitted REP. Fig. 8(a) is a histogram of R calculated for the 24 tubes. As expected, the measured RBM REP line shapes are symmetric [27].

Finally, Fig. 8(b) presents a histogram of the broadening parameters η measured from 24 tubes. The minimum η value we observed is 8.8 meV, similar to the only previously reported REP measurement of one single tube on a Si substrate [33]. Interestingly, it seems like the nanotubes that appear in small bundles have a narrower broadening than that of an individual nanotube. This result can be contrasted with the measurements from large bundles where the resonant profile is very broad ($\eta \sim 120$ meV) [17]. The larger line widths of the REPs in large bundles, where many resonant nanotubes contribute, are likely due to inhomogeneous broadening.

VI. CONCLUSION

The van Hove singularities in the DOS, typical of 1-D structures, make it possible to measure the normally weak Raman signal from a single carbon nanotube. We have demonstrated spatial mapping of carbon nanotubes using the resonant signature; measured the REP that determines the optical transition energy with meV precision as well as finding information about the lifetime of the intermediate states via the broadening factor. In short, resonant Raman scattering provides a wealth of information about the vibronic and electronic properties of SWNTs.

ACKNOWLEDGMENT

The authors acknowledge helpful discussions with A. Castro-Neto, F. Guinea, and M. Dresselhaus.

REFERENCES

[1] R. Saito, G. Dresselhaus, and M. S. Dresselhaus, *Physical Properties of Carbon Nanotubes*, 1st ed. Singapore: World Scientific, 1998.

[2] S. Reich, C. Thomsen, and J. Maultzsch, *Carbon Nanotubes: Basic Concepts and Physical Properties*. New York: Wiley–VCH, 2004.

[3] M. J. O'Connell, S. M. Bachilo, C. B. Huffman, V. C. Moore, M. S. Strano, E. H. Haroz, K. L. Rialon, P. J. Boul, W. H. Noon, C. Kittrell, J. P. Ma, R. H. Hauge, R. B. Weisman, and R. E. Smalley, "Band gap fluorescence from individual single-walled carbon nanotubes," *Science*, vol. 297, pp. 593–596, 2002.

[4] F. Wang, G. Dukovic, L. E. Brus, and T. F. Heinz, "Time-resolved fluorescence of carbon nanotubes and its implication for radiative lifetimes," *Phys. Rev. Lett.*, vol. 92, pp. 177401–177404, 2004.

[5] S. M. Bachilo, M. S. Strano, C. Kittrell, R. H. Hauge, R. E. Smalley, and R. B. Weisman, "Structure-assigned optical spectra of single-walled carbon nanotubes," *Science*, vol. 298, pp. 2361–2366, 2002.

[6] J. Maultzsch, R. Pomraenke, S. Reich, E. Chang, D. Prezzi, A. Ruini, E. Molinari, M. S. Strano, C. Thomsen, and C. Lienau, "Exciton binding energies in carbon nanotubes from two-photon photoluminescence," *Phys. Rev. B*, vol. 72, pp. 241402–241405, 2005.

[7] F. Wang, G. Dukovic, L. E. Brus, and T. F. Heinz, "The optical resonances in carbon nanotubes arise from excitons," *Science*, vol. 308, pp. 838–841, 2005.

[8] T. Ando, "Excitons in carbon nanotubes," *J. Phys. Soc. Jpn.*, vol. 66, pp. 1066–1073, 1997.

[9] C. L. Kane and E. J. Mele, "Ratio problem in single carbon nanotube fluorescence spectroscopy," *Phys. Rev. Lett.*, vol. 90, pp. 207401–207404, 2003.

[10] P. Y. Yu and M. Cardona, *Fundamentals of Semiconductors: Physics and Materials Properties*, 3rd ed. Berlin, Germany: Springer, 2005.

[11] T. Ogawa and T. Takagahara, "Optical-absorption and Sommerfeld factors of one-dimensional semiconductors—An exact treatment of excitonic effects," *Phys. Rev. B*, vol. 44, pp. 8138–8156, 1991.

[12] M. S. Dresselhaus, G. Dresselhaus, R. Saito, and A. Jorio, "Raman spectroscopy of carbon nanotubes," *Phys. Rep. Rev. Sect. Phys. Lett.*, vol. 409, pp. 47–99, 2005.

[13] S. B. Cronin, A. K. Swan, M. S. Unlu, B. B. Goldberg, M. S. Dresselhaus, and M. Tinkham, "Measuring the uniaxial strain of individual single-wall carbon nanotubes: Resonance Raman spectra of atomic-force-microscope modified single-wall nanotubes," *Phys. Rev. Lett.*, vol. 93, pp. 167401–167404, 2004.

[14] S. B. Cronin, Y. Yin, A. Walsh, R. B. Capaz, A. Stolyarov, P. Tangney, M. L. Cohen, S. G. Louie, A. K. Swan, M. S. Unlu, B. B. Goldberg, and M. Tinkham, "Temperature dependence of the optical transition energies of carbon nanotubes: The role of electron—phonon coupling and thermal expansion," *Phys. Rev. Lett.*, vol. 96, pp. 127403–127406, 2006.

[15] J. Lefebvre, P. Finnie, and Y. Homma, "Temperature-dependent photoluminescence from single-walled carbon nanotubes," *Phys. Rev. B*, vol. 70, pp. 045419–045426, 2004.

[16] J. Lefebvre, J. M. Fraser, Y. Homma, and P. Finnie, "Photoluminescence from single-walled carbon nanotubes: A comparison between suspended and micelle-encapsulated nanotubes," *Appl. Phys. A Mater. Sci. Process.*, vol. 78, pp. 1107–1110, 2004.

[17] C. Fantini, A. Jorio, M. Souza, M. S. Strano, M. S. Dresselhaus, and M. A. Pimenta, "Optical transition energies for carbon nanotubes from resonant Raman spectroscopy: Environment and temperature effects," *Phys. Rev. Lett.*, vol. 93, pp. 147406–147409, 2004.

[18] V. C. Moore, M. S. Strano, E. H. Haroz, R. H. Hauge, R. E. Smalley, J. Schmidt, and Y. Talmon, "Individually suspended single-walled carbon nanotubes in various surfactants," *Nano Lett.*, vol. 3, pp. 1379–1382, 2003.

[19] H. Telg, J. Maultzsch, S. Reich, F. Hennrich, and C. Thomsen, "Chirality distribution and transition energies of carbon nanotubes," *Phys. Rev. Lett.*, vol. 93, pp. 177401–177404, 2004.

[20] S. K. Doorn, D. A. Heller, P. W. Barone, M. L. Usrey, and M. S. Strano, "Resonant Raman excitation profiles of individually dispersed single walled carbon nanotubes in solution," *Appl. Phys. A Mater. Sci. Process.*, vol. 78, pp. 1147–1155, 2004.

[21] Y. Yin, A. Vamivakas, A. Walsh, S. Cronin, M. S. Ünlü, B. B Goldberg, and A. K. Swan, "Optical determination of electron–phonon coupling in carbon nanotubes," arXiv.org:cond-mat/0605670, *Phys. Rev. Lett.* submitted for publication.

[22] A. Jorio, M. A. Pimenta, A. G. Souza, R. Saito, G. Dresselhaus, and M. S. Dresselhaus, "Characterizing carbon nanotube samples with resonance Raman scattering," *N. J. Phys.*, vol. 5, pp. 139.1–139.17, 2003.

[23] J. C. Meyer, M. Paillet, T. Michel, A. Moreac, A. Neumann, G. S. Duesberg, S. Roth, and J. L. Sauvajol, "Raman modes of index-identified freestanding single-walled carbon nanotubes," *Phys. Rev. Lett.*, vol. 95, pp. 217401–217404, 2005.

[24] R. M. Martin and L. M. Falicov, *Light Scattering in Solids I*. Ch. 3, vol. 8. Berlin: Springer, 1983, pp. 79–95.

[25] A. Hartschuh, E. J. Sanchez, X. S. Xie, and L. Novotny, "High-resolution near-field Raman microscopy of single-walled carbon nanotubes," *Phys. Rev. Lett.*, vol. 90, pp. 95503–95506, 2003.

[26] A. N. Vamivakas, A. Walsh, Y. Yin, M. S. Unlu, B. B. Goldberg, and A. K. Swan, "Exciton mediated one phonon resonant Raman scattering from one dimensional systems," *Phys. Rev. B*, to be published (arXiv.org:cond-mat/0604515).

[27] M. Canonico, G. B. Adams, C. Poweleit, J. Menendez, J. B. Page, G. Harris, H. P. van der Meulen, J. M. Calleja, and J. Rubio, "Characterization of carbon nanotubes using Raman excitation profiles," *Phys. Rev. B*, vol. 65, pp. 201402–201405, 2002.

[28] B. Richards and E. Wolf, "Electromagnetic diffraction in optical systems. II: Structure of the image field in an aplanatic system," *Proc. R. Soc. A*, vol. 253, pp. 358–379, 1959.

[29] A. G. Souza Filho, S. G. Chou, G. G. Samsonidze, G. Dresselhaus, M. S. Dresselhaus, L. An, J. Liu, A. K. Swan, M. S. Unlu, B. B. Goldberg, A. Jorio, A. Gruneis, and R. Saito, "Stokes and anti-Stokes Raman spectra of small-diameter isolated carbon nanotubes," *Phys. Rev. B*, vol. 69, pp. 115428–115436, 2004.

[30] Y. Homma, Y. Kobayashi, T. Ogino, and T. Yamashita, "Growth of suspended carbon nanotube networks on 100-nm-scale silicon pillars," *Appl. Phys. Lett.*, vol. 81, pp. 2261–2263, 2002.

[31] M. S. Strano, "Probing chiral selective reactions using a revised Kataura plot for the interpretation of single-walled carbon nanotube spectroscopy," *J. Amer. Chem. Soc.*, vol. 125, pp. 16148–16153, 2003.

[32] F. Wang, M. Y. Sfeir, L. Huang, X. M. H. Huang, Y. Wu, J. Kim, J. Hone, S. O'Brien, L. E. Brus, and T. F. Heinz, "Interactions between individual carbon nanotubes studied by Rayleigh scattering spectroscopy," *Phys. Rev. Lett.*, vol. 96, 167401, 2006.

[33] A. Jorio, A. G. Souza, G. Dresselhaus, M. S. Dresselhaus, R. Saito, J. H. Hafner, C. M. Lieber, F. M. Matinaga, M. S. S. Dantas, and M. A. Pimenta, "Joint density of electronic states for one isolated single-wall carbon nanotube studied by resonant Raman scattering," *Phys. Rev. B*, vol. 6324, pp. 245416–245419, 2001.

Yan Yin (S'03) received the B.S. degree in physics and electronics and information systems Boston University, Boston, MA, in 2006, and the M.S. degree in physics from Peking University, Beijing, China, in 1997 and 1999, respectively. He received the Ph.D. degree from Boston University, Boston, MA, in May 2006. His dissertation topic focused on the resonant Raman scattering excitation and photoluminescence excitation studies of carbon nanotubes.

His current research interests include, but are not restricted to, near-field optics, photonics and optoelectronic devices, and optical spectroscopy applications for nano-science and nanotechnology.

Mr. Yin is a student member of the Materials Research Society and American Physical Society.

Andy G. Walsh received the B.S. degree from Cornell University, Ithaca, NY, in 1992. He is currently working toward the Ph.D. degree in physics at Boston University, Boston, MA.

He worked as a Naval Officer for ten years, when he flew the H-46 Sea Knight and administered the network at the Naval Academy Preparatory School. His current research interests include nano-scale spectroscopy and characterization of the electronic and vibrational properties of carbon nanotubes.

A. Nick Vamivakas received the M.S. degree in electrical engineering in 2003 from Boston University, Boston, MA, where he is currently working toward the Ph.D. degree in electrical engineering.

His current research interests include nano-scale spectroscopy.

Stephen B. Cronin received the Ph.D. degree in physics from Massachusetts Institute of Technology, Cambridge, in 2002, under advisor Prof. Mildred Dresselhaus.

From 2002 to 2005, he received the post-doctoral training at the Department of Physics, Harvard University, where he worked under Prof. Michael Tinkham. He is currently a Faculty Member in the Department of Electrical Engineering–Electrophysics, University of Southern California, Los Angeles, CA. His current research interests include Raman spectroscopy and transport measurements of individual carbon nanotubes.

Alexander (Sasha) M. Stolyarov received the B.S. degree in physics from the University of Texas, Dallas, in 2005. He is currently working toward the Ph.D. degree in applied physics at Harvard University, Cambridge, MA.

During the summer and fall of the undergraduate senior year, he joined Professor Michael Tinkham's group at Harvard University, where his research activities focused on the fabrication and measurement of carbon nanotube devices.

Michael Tinkham received the Ph.D. degree in physics in 1954.

He is the Rumford Professor of Physics and Gordon McKay Professor of Applied Physics at Harvard University, Cambridge, MA. His research has focused on superconductivity for many years. In recent years, he has been particularly active in studying the unique properties of materials when sample dimensions are reduced to the nanometer range. Such studies are motivated both by their intrinsic scientific interest and by their potential importance in finding new ways to fabricate ultracompact electronic components on a molecular size scale. His current research interests include transport properties of superconducting nanowires and single-walled carbon nanotubes.

Wolfgang Bacsa is a Professor of physics at Universite Paul Sabatier, Toulouse, France. He spent a sabbatical year at Boston University from 2004 to 2005. He has extensive optical and spectroscopic expertise. His current research interests include inelastic light scattering in low-dimensional and strongly correlated electron systems and synthesis of carbon nanotubes and their optical, electronic, and magnetic properties.

M. Selim Ünlü (S'90–M'91–SM'95) was born in Sinop, Turkey, in 1964. He received the B.S. degree in electrical engineering from the Middle East Technical University, Ankara, Turkey, in 1986. He received the M.S.E.E. and Ph.D. degrees from the University of Illinois, Urbana-Champaign, in 1988 and 1992, respectively, both in electrical engineering. His dissertation topic dealt with the resonant cavity enhanced (RCE) photodetectors and optoelectronic switches.

In 1992, he joined Boston University, Boston, MA, as an Assistant Professor. Currently, he is a Professor in the Department of Electrical and Computer Engineering, Boston University. From January to July 2000, he was a Visiting Professor at the University of Ulm, Ulm, Germany. His current research interests include research and development of photonic materials, devices and systems focusing on the design, processing, characterization, and modeling of semiconductor optoelectronic devices, especially photodetectors. His current specific interests and expertise include high-speed RCE photodetectors, time and spatially resolved optical characterization of semiconductor materials, near-field and picosecond spectroscopy, near-field imaging of laser diodes, photonic bandgap and guided-wave devices, solid immersion lens microscopy, thermal imaging, biosensor fabrication and development of waveguide evanescent bio-imaging techniques, and hyperpolarized noble gas MRI. He is the author or coauthor of more than 150 technical articles and several book chapters and magazine articles. He has edited one book and holds one U.S. patent. He also has several patents pending.

Dr. Ünlü served as the Chair of IEEE Laser and Electro-Optics Society (LEOS), Boston Chapter, winning the LEOS Chapter-of-the-Year Award, during 1994 and 1995. He served as the Vice President of SPIE New England Chapter from 1998 to 1999. He was awarded National Science Foundation Research Initiation Award in 1993, United Nations TOKTEN Award in 1995 and 1996, and both the National Science Foundation CAREER and Office of Naval Research Young Investigator Awards in 1996. During 1999 to 2001, he served as the Chair of the IEEE/LEOS Technical Subcommittee on Photodetectors and Imaging. Currently, he is an Associate Editor of IEEE JOURNAL OF QUANTUM ELECTRONICS.

Bennett B. Goldberg (M'05) received the B.A. degree in physics from Harvard University, Cambridge, MA, in 1982. He received the M.S. and Ph.D. degrees in physics from Brown University, Providence, RI, in 1984 and 1987, respectively.

He worked as a Bantrell Post-Doctoral Fellow at Massachusetts Institute of Technology and the Francis Bitter National Magnet Laboratory. In 1989, he joined the Physics Faculty, Boston University, Boston, MA, where he is a Professor of physics, electrical and computer engineering, and biomedical engineering. Currently, he is the Chairman of the Physics Department, Boston University. He is the Director of Boston University's new Center for Nanoscience and Nanobiotechnology, an interdisciplinary center that brings together academic and industrial scientists and engineers in the development of nanotechnology with applications in materials and biomedicine. His current research interests include the general area of ultra-high resolution microscopy and spectroscopy techniques for hard and soft materials systems. He has worked in the field of near-field imaging of photonic bandgap, ring microcavity, and single-mode waveguide devices, and has recently developed subsurface solid immersion microscopy for Si inspection. His group is working on novel approaches to subcellular imaging with interferometric fluorescenent techniques, and in biosensor fabrication and development of waveguide evanescent bio-imaging techniques. His nano-optics research includes Raman scattering of individual nanotubes and nano-optics of electron systems in quantum wells and quantum dot structures.

Anna K. Swan (M'05) received the M.S. degree in physics engineering from Chalmers University, Gothenburg, Sweden, in 1986, and the Ph.D. degree in physics from Boston University, Boston, MA, in 1993.

She was a Wigner Fellow in the Solid State Division at Oak Ridge National Laboratory. She joined the Electrical and Computer Engineering Department, Boston University, as a Research Assistant Professor, in 1999, where she is currently an Associate Professor. Her current research interests include high spatial resolution spectroscopy of single carbon nanotubes and spectral self-interference as a means of improving fluorescence microscopy resolution for biological imaging.

Dr. Swan received two student awards, the Nottingham Prize and the Morton M. Traum Award, for her dissertation on spin-ordering on NiO(1 0 0) surfaces using metastable He* scattering.